Acta Crystallographica Section F
Structural Biology and Crystallization Communications
ISSN 1744-3091

Purification, crystallization and preliminary X-ray diffraction experiments on the breakage-reunion domain of the DNA gyrase from *Mycobacterium tuberculosis*

Jérémie Piton,[a] Stéphanie Matrat,[b] Stéphanie Petrella,[c] Vincent Jarlier,[b] Alexandra Aubry[b] and Claudine Mayer[a]*

[a]Unité de Dynamique Structurale des Macromolécules, Département de Biologie Structurale et Chimie, URA 2185 du CNRS, Institut Pasteur, France, [b]UPMC Université Paris 06, EA1541, Laboratoire de Bactériologie-Hygiène, France, and [c]INSERM U872–LRMA, Equipe 12, Centre de Recherche des Cordeliers, France

Correspondence e-mail: mayer@pasteur.fr

Received 31 August 2009
Accepted 13 October 2009

Mycobacterium tuberculosis DNA gyrase, a nanomachine that is involved in the regulation of DNA topology, is the only type II topoisomerase present in this organism and hence is the sole target for fluoroquinolone action. The breakage-reunion domain of the A subunit plays an essential role in DNA binding during the catalytic cycle. Two constructs of 53 and 57 kDa (termed GA53BK and GA57BK) corresponding to this domain have been overproduced, purified and crystallized. Diffraction data were collected from four crystal forms. The resolution limits ranged from 4.6 to 2.7 Å depending on the crystal form. The best diffracting crystals belonged to space group *C*2, with a biological dimer in the asymmetric unit. This is the first report of the crystallization and preliminary X-ray diffraction analysis of the breakage-reunion domain of DNA gyrase from a species containing one unique type II topoisomerase.

1. Introduction

Mycobacterium tuberculosis is the aetiological agent of tuberculosis (TB) and remains one of the most damaging human pathogens. It is estimated to have infected nearly a third of the world population and is responsible for the loss of two million lives every year according to the World Health Organization (WHO; http://www.who.int). *M. tuberculosis* is intrinsically resistant to the majority of available antibiotics (Morris *et al.*, 2005). Moreover, the increasing incidence of multidrug-resistant tuberculosis (MDR-TB), which involves bacilli that are resistant to the two main anti-TB drugs, isoniazid and rifampicin, is a worldwide problem and makes the control of tuberculosis difficult. Fluoroquinolones are some of the rare effective second-line drugs that are active against *M. tuberculosis* (Aubry *et al.*, 2004) and are nowadays part of the treatment recommended for MDR-TB (WHO; Veziris *et al.*, 2003). Unfortunately, the increasing use of quinolones in the treatment of TB can lead to decreased quinolone susceptibility in *M. tuberculosis*. The structural bases and detailed molecular mechanisms of quinolone action and resistance in this organism are still unknown.

Quinolones target the bacterial type II topoisomerases, DNA gyrase and topoisomerase IV, which are two related ATP-dependent enzymes that act *via* a double-stranded DNA break (Champoux, 2001) and act in unison to facilitate DNA replication and chromosome segregation at cell division. DNA gyrase and topoisomerase IV are structurally and mechanistically related but have acquired distinct characteristics during evolution (Champoux, 2001). DNA gyrase facilitates DNA unwinding at replication forks and topoisomerase IV has a specialized function in mediating the decatenation of interlocked daughter chromosomes (Champoux, 2001; Levine *et al.*, 1998). As the *M. tuberculosis* genome encodes only one type II topoisomerase, DNA gyrase (Cole *et al.*, 1998), it has become the sole target in tuberculosis treatment. This enzyme consists of two subunits, GyrA and GyrB, encoded by the *gyrA* and *gyrB* genes, respectively, which form a catalytically active heterotetrameric (A_2B_2) complex. Subunit A consists of two domains: an N-terminal breakage-reunion domain and a carboxy-terminal domain (CTD). Subunit B consists of

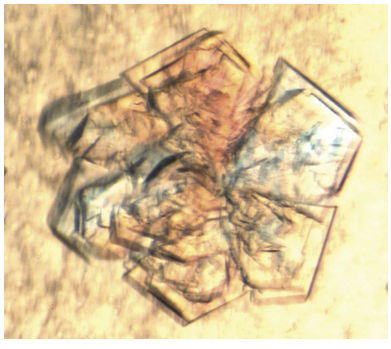

Table 1
Description of the four crystal forms obtained with the two constructs.

	GA53BK		GA57BK	
	Form I	Form II	Form III	Form IV
Temperature (K)	293	293	293	293
Crystal-growth time	1 week	2 d	2 weeks	2–4 d
Crystallization solution	0.1 *M* sodium cacodylate pH 6.5, 0.01 *M* magnesium acetate, 1.3 *M* lithium sulfate	0.1 *M* bicine pH 9, 0.15 *M* sodium chloride, 4%(*w*/*v*) PEG 550 MME	0.1 *M* Na HEPES pH 7.5, 0.2 *M* calcium chloride, 22%(*w*/*v*) PEG 400	0.1 *M* Na HEPES pH 7.5, 4%(*w*/*v*) PEG 4000, 30%(*v*/*v*) MPD
Crystal dimensions (µm)	60 × 60 × 60	300 × 30 × 30	150 × 100 × 100	200 × 200 × 20
Space group	*I*23	$P6_12_12$	$C222_1$	*C*2
Unit-cell parameters (Å, °)	$a = b = c = 327.2$, $\alpha = \beta = \gamma = 90$	$a = b = 196.2$, $c = 281.8$, $\alpha = \beta = 90$, $\gamma = 120$	$a = 89.5$, $b = 187.4$, $c = 149.0$, $\alpha = \beta = \gamma = 90$	$a = 163.9$, $b = 109.6$, $c = 102.0$, $\alpha = \gamma = 90$, $\beta = 120.4$
Unit-cell volume (Å^3)	35×10^6	9×10^6	2.5×10^6	1.6×10^6
No. of asymmetric units (ASUs) in cell	24	12	8	2
Range of possible No. of molecules in ASU	5–14	3–8	1–3	1–4
No. of molecules in ASU	6	3	2	2
V_M (Å^3 Da^{-1})	4.58	4.88	2.72	3.44
Solvent content (%)	73.15	74.81	54.76	64.26
No. of biological units in ASU	3	1.5	1	1
No. of crystals tested	50	100	20	20
Resolution limit (Å)	4.6	4.0	3.4	2.7

an ATPase domain and a TOPRIM domain (reviewed by Schoeffler & Berger, 2008). The enzyme core is cooperatively formed by the GyrA breakage-reunion and GyrB TOPRIM domains.

The main mechanism currently known to be responsible for *M. tuberculosis* quinolone resistance arises from mutations in DNA gyrase (Mdluli & Ma, 2007). Most mutations that confer bacterial resistance to quinolones occur in a short discrete segment termed the quinolone resistance-determining region (QRDR; Takiff *et al.*, 1994) in the breakage-reunion domain of the GyrA subunit or, more rarely, in the TOPRIM domain of GyrB. These two regions are most likely to be the site of quinolone interaction and are also the DNA-binding site, as confirmed by the recent first structure of a subdomain of a eukaryotic type II topoisomerase in complex with DNA (Dong & Berger, 2007). The first picture at a molecular level of a type II topoisomerase–quinolone–DNA complex revealed that the quinolone is intercalated at the protein–DNA interface (Laponogov *et al.*, 2009).

As *M. tuberculosis* uses only one type II topoisomerase to ensure the regulation of DNA superhelical density, the *M. tuberculosis* enzyme exhibits a different activity spectrum compared with other DNA gyrases, *e.g.* it supercoils DNA with an efficiency comparable to those of other DNA gyrases but shows enhanced relaxation, DNA cleavage and decatenation activities (Aubry *et al.*, 2006). Mycobacterial DNA gyrase displays high sequence similarity to other DNA gyrases, for example 44% identity (65% similarity) to *Escherichia coli* DNA gyrase, the only breakage-reunion domain of a DNA gyrase for which the structure is known (Morais-Cabral *et al.*, 1997). Knowledge of how the three-dimensional structure and sequence–structure relationships play a role in this functional specificity will need a better understanding of the protein–DNA interactions at the atomic level. In this communication, we report the crystallization and preliminary X-ray diffraction analysis of the breakage-reunion domain of DNA gyrase from *M. tuberculosis*, a species containing one unique type II topoisomerase.

2. Materials and methods

2.1. Cloning, overproduction and purification

Two constructs were designed for the breakage-reunion domain of *M. tuberculosis* H37Rv *gyrA*, a long construct containing residues Met1–Ile498 (*ga57bk*) and a short construct containing residues Val37–Ile498 (*ga53bk*). This led to the generation of proteins with molecular masses of approximately 53 kDa (GA53BK) and 57 kDa (GA57BK), respectively. The cloning, overproduction and purification protocols were exactly the same for the two constructs. PCR products were ligated into the pMOS Blue plasmid (GE Healthcare) and transformed into *Escherichia coli* MosBlue competent cells according to the manufacturer's instructions. Recombinant plasmids were recovered from the white colonies and digested with *Nde*I and *Xho*I and the DNA fragments obtained were ligated into *Nde*I-*Xho*I-cut pET-29a (Novagen) and transformed into *E. coli* Rosetta (DE3) pLysS (Novagen). Cells freshly transformed with pET29a/*ga53bk* or pET29a/*ga57bk* were grown at 310 K overnight in LB medium containing 50 µg ml^{-1} kanamycin and 40 µg ml^{-1} chloramphenicol. At an OD_{600} of 0.6, IPTG was added to a final concentration of 1 m*M* and the cells were grown at 293 K overnight. Following harvesting, the cell pellet was resuspended in binding buffer (20 m*M* Tris–HCl pH 8.0, 300 m*M* NaCl and 20 m*M* imidazole) and lysed by sonication. The cell lysate obtained by centrifugation at 27 000*g* for 1 h was loaded directly onto an Ni–NTA column (GE Healthcare) which was pre-equilibrated with binding buffer. The column was washed with wash buffer (20 m*M* Tris–HCl pH 8.0, 300 m*M* NaCl, 50 m*M* imidazole). Recombinant protein with a His_6 tag at the C-terminus was eluted with elution buffer (20 m*M* Tris–HCl pH 8.0, 300 m*M* NaCl, 300 m*M* imidazole). All Ni–NTA affinity-chromatography steps were performed at 277 K. The protein was concentrated using Vivapore concentrators and then injected onto a Superdex 75 HR 10/30 gel-filtration column (GE Healthcare) pre-equilibrated in 20 m*M* Tris–HCl pH 8.

2.2. Crystallization, data collection and processing

The GA53BK and GA57BK proteins were concentrated to 9 and 15 mg ml^{-1}, respectively, in 20 m*M* Tris–HCl pH 8. Initial crystallization trials were performed using several commercial screens: MDL from Molecular Dimensions, Wizard I, Wizard II and JBS 1–8 from Jena Bioscience and Crystal Screen I, Crystal Screen II, Cryo, Natrix and PEG/Ion from Hampton Research. After screening, the crystallization conditions were optimized by varying the salt and the crystallizing agent concentrations using the vapour-diffusion method in hanging drops by mixing 2 µl protein solution and 1 µl reservoir solution. Crystals were mounted in a cryoloop and flash-cooled in

Table 2
Data-collection statistics for the four crystal forms.

Values in parentheses are for the highest resolution shell.

	GA53BK form I	GA53BK form II	GA57BK form III	GA57BK form IV
X-ray source	ID23-eh2	SOLEIL PROXIMA 1	SOLEIL PROXIMA 1	SOLEIL PROXIMA 1
Space group	$I23$	$P6_12_12$	$C222_1$	$C2$
Unit-cell parameters (Å, °)	$a = b = c = 327.2$	$a = b = 196.2$, $c = 281.8$	$a = 89.5$, $b = 187.4$, $c = 149.0$	$a = 163.9$, $b = 109.6$, $c = 102.0$, $\beta = 120.4$
Wavelength (Å)	0.98	0.98	0.98	0.98
Resolution range (Å)	35–4.6 (4.8–4.6)	35–4.0 (4.2–4.0)	35–3.4 (3.6–3.4)	35–2.7 (2.8–2.7)
No. of observations	147454 (23253)	198444 (27348)	97456 (14819)	146716 (4383)
Unique reflections	32382 (5108)	27390 (3677)	17425 (2673)	42470 (4283)
Completeness (%)	99.6 (98.5)	99.7 (99.2)	98.6 (95.7)	99.9 (98)
Redundancy	4.55 (4.52)	7.2 (7.2)	6.5 (6.5)	3.5 (3.5)
$\langle I/\sigma(I)\rangle$	8.83 (3.12)	8.78 (2.43)	10.75 (2.79)	12.44 (2.24)
$R_{\rm merge}$† (%)	17.1 (50.6)	19.8 (66.3)	14.2 (62.1)	8.6 (72.6)

† $R_{\rm merge} = \sum_{hkl}\sum_i |I_i(hkl) - \langle I(hkl)\rangle| / \sum_{hkl}\sum_i I_i(hkl)$, where $I_i(hkl)$ is the intensity of an individual reflection and $\langle I(hkl)\rangle$ is its mean value.

liquid nitrogen in the presence of 25% glycerol when necessary. The best and largest single crystals were used for data collection.

X-ray diffraction data were collected at 100 K on beamlines ID23-2 of the European Synchrotron Radiation Facility, Grenoble and PROXIMA 1 of the SOLEIL synchrotron, Saint-Aubin. Data were processed with *XDS* (Kabsch, 1988) and scaling was performed with *SCALA* from the *CCP*4 program suite (v.6.1.1; Collaborative Computational Project, Number 4, 1994).

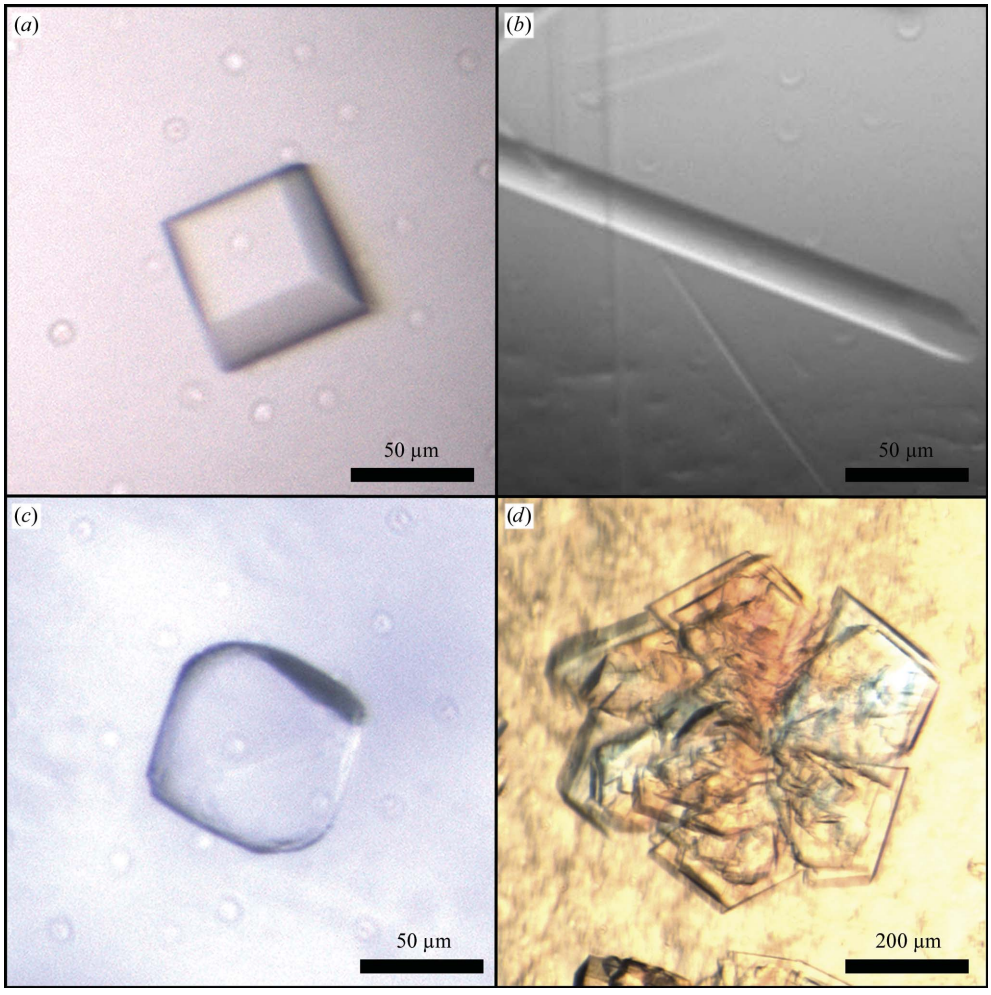

Figure 1
(*a*) Crystal form I of GA53BK obtained in 100 m*M* sodium cacodylate pH 6.5, 10 m*M* magnesium acetate and 1.3 *M* lithium sulfate. After one week, the crystal size was 60 × 60 × 60 µm. (*b*) Crystal form II of GA53BK obtained in 100 m*M* bicine pH 9, 150 m*M* sodium chloride, 9% PEG 550 MME and 9% ethylene glycol. After 2 d, the crystal size was 300 × 30 × 30 µm. (*c*) Crystal form III of GA57BK obtained in 100 m*M* Na HEPES pH 7.5, 200 m*M* calcium chloride and 22% PEG 400. After two weeks, the crystal size was 150 × 100 × 100 µm. (*d*) Crystal form IV of GA57BK obtained in 100 m*M* HEPES pH 7.5, 4% PEG 4000 and 30% MPD. After 2 d, the crystal size was 200 × 40 × 40 µm. One single crystal was isolated to collect the complete data set described in Table 2.

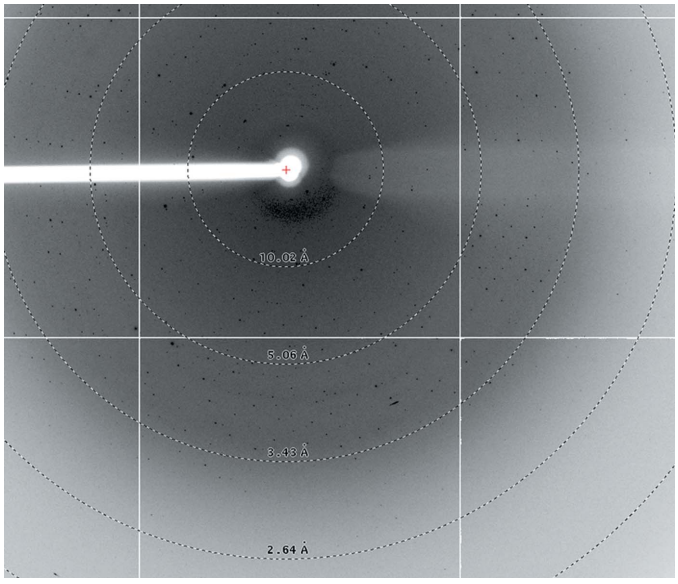

Figure 2
Typical X-ray diffraction pattern of crystal form IV. The oscillation angle was 0.5°.

2.3. Molecular replacement and refinement

Molecular replacement calculations were performed with *AMoRe* (Navaza, 1994) and *MOLREP* (Vagin & Teplyakov, 1997) as implemented in the *CCP*4 suite using the structures of various breakage-reunion domains of type II topoisomerases, namely *E. coli* DNA gyrase (PDB code 1ab4; Morais Cabral *et al.*, 1997) and topoisomerase IV (PDB code 1zvu; Corbett *et al.*, 2005), *Streptococcus pneumoniae* topoisomerase IV (PDB code 2nov; Laponogov *et al.*, 2007) and yeast topoisomerase II (PDB code 1bgw; Berger *et al.*, 1996). The best hits were obtained with the *E. coli* DNA gyrase structure. Refinement was performed with *REFMAC*5 (Murshudov *et al.*, 1997) and *BUSTER* (Blanc *et al.*, 2004); electron-density maps were calculated and analyzed with *Coot* (Emsley & Cowtan, 2004).

3. Results and discussion

The GA53BK construct was designed based on the structure of the breakage-reunion domain of *E. coli*, in which the first 30 N-terminal amino acids are not visible in the electron density. GA53BK and GA57BK were 99% pure as estimated by SDS–PAGE after two steps of purification: an affinity His-trap purification followed by a gel-filtration step. Both proteins eluted from the Superdex 75 size-exclusion chromatography column with an apparent molecular mass corresponding to a dimer.

High-throughput screening of initial crystallization conditions for the two constructs resulted in several hits. Initial optimization experiments for each hit yielded crystals with different morphologies which diffracted X-ray radiation to about 4.5 Å resolution. After extensive optimization of the crystallization conditions, crystals suitable for diffraction experiments were obtained in four different conditions (Table 1 and Fig. 1) corresponding to four distinct crystal forms: two for GA53BK (forms I and II) and two for GA57BK (forms III and IV). For each crystal form, numerous crystals were tested (Table 1), resulting in the conclusion that forms I and II obtained for GA53BK are limited to 4.6 and 4.0 Å resolution, respectively (Table 2). Whereas crystals of form I mainly diffracted to 6–8 Å resolution, with very few crystals diffracting to above 5 Å, all form II crystals tested diffracted to about 4–5 Å resolution. Most form III crystals exhibited diffraction patterns that were very close to powder diffraction. Only one of the 20 crystals tested diffracted to about 3.5 Å resolution. In contrast, all form IV crystals diffracted X-ray radiation to above 3 Å resolution. For each crystal form, a complete data set was collected to the diffraction limit (Tables 1 and 2). In conclusion, the best diffracting crystal was obtained for form IV in 0.1 *M* Na HEPES pH 7.5, 4%(*w*/*v*) PEG 4000 and 30%(*v*/*v*) MPD and resulted in a complete diffraction data set to 2.7 Å resolution in space group *C*2 (Fig. 2 and Table 2).

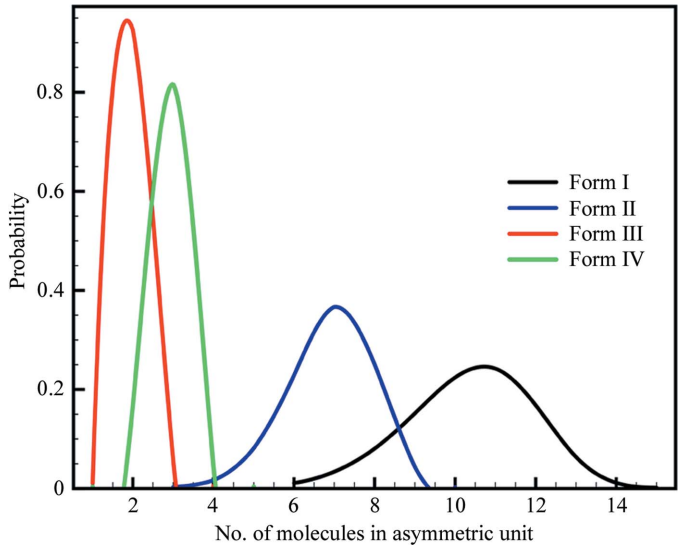

Figure 3
Probability distributions (Kantardjieff & Rupp, 2003) of the different possible numbers of molecules in the asymmetric unit for the four crystal forms.

Matthews coefficient (Matthews, 1968) calculations for the two forms of GA53BK show that form I could contain 5–14 copies of the construct per asymmetric unit and form II two to eight copies (Fig. 3). Molecular replacement for these two forms using the truncated breakage-reunion domain of *E. coli* DNA gyrase revealed six and three copies, respectively, corresponding to 75% solvent content. This high solvent content could explain the resolution limit of 4 Å (Heras & Martin, 2005). Molecular replacement was performed for forms III and IV as described previously for GA53BK. Both crystal forms contained two copies of the construct, which corresponds to the biological dimer (as observed by gel-filtration chromatography). Matthews coefficient calculations with two copies correspond to 55 and 64% solvent content for the two forms, respectively. A self-rotation function revealed the presence of the twofold NCS that relates the two monomers of the biological dimer. As the DNA gyrase dimers of the four crystal forms possessed a similar conformation, we concentrated on crystal form IV. The structure of this crystal form has been refined and will be published elsewhere. The coordinates have been deposited in the Protein Data Bank under accession code 3ifz.

We would like to thank David Flot from EMBL at the ESRF (Grenoble), Andrew Thompson at SOLEIL (Saint-Aubin) for assistance during data collection and Ahmed Haouz from the crystallogenesis Platform at the Pasteur Institute. We also thank Hugues Nury and Marc Delarue for helpful discussions.

References

Aubry, A., Fisher, L. M., Jarlier, V. & Cambau, E. (2006). *Biochem. Biophys. Res. Commun.* **348**, 158–165.

Aubry, A., Pan, X. S., Fisher, L. M., Jarlier, V. & Cambau, E. (2004). *Antimicrob. Agents Chemother.* **48**, 1281–1288.
Berger, J. M., Gamblin, S. J., Harrison, S. C. & Wang, J. C. (1996). *Nature (London)*, **379**, 225–232.
Blanc, E., Roversi, P., Vonrhein, C., Flensburg, C., Lea, S. M. & Bricogne, G. (2004). *Acta Cryst.* D**60**, 2210–2221.
Champoux, J. J. (2001). *Annu. Rev. Biochem.* **70**, 369–413.
Cole, S. T. *et al.* (1998). *Nature (London)*, **393**, 515–516.
Collaborative Computational Project, Number 4 (1994). *Acta Cryst.* D**50**, 760–763.
Corbett, K. D., Schoeffler, A. J., Thomsen, N. D. & Berger, J. M. (2005). *J. Mol. Biol.* **351**, 545–651.
Dong, K. C. & Berger, J. M. (2007). *Nature (London)*, **450**, 1201–1205.
Emsley, P. & Cowtan, K. (2004). *Acta Cryst.* D**60**, 2126–2132.
Heras, B. & Martin, J. L. (2005). *Acta Cryst.* D**61**, 1173–1180.
Kabsch, W. (1988). *J. Appl. Cryst.* **21**, 67–72.
Kantardjieff, K. A. & Rupp, B. (2003). *Protein Sci.* **12**, 1865–1871.
Laponogov, I., Sohi, M. K., Veselkov, D. A., Pan, X. S., Sawhney, R., Thompson, A. W., McAuley, K. E., Fisher, L. M. & Sanderson, M. R. (2009). *Nature Struct. Mol. Biol.* **16**, 667–669.
Laponogov, I., Veselkov, D. A., Sohi, M. K., Pan, X. S., Achari, A., Yang, C., Ferrara, J. D., Fisher, L. M. & Sanderson, M. R. (2007). *PLoS One*, **2**, e301.
Levine, C., Hiasa, H. & Marians, K. J. (1998). *Biochem. Biophys. Acta*, **1400**, 29–43.
Matthews, B. W. (1968). *J. Mol. Biol.* **33**, 491–497.
Mdluli, K. & Ma, Z. (2007). *Infect. Disord. Drug Targets*, **7**, 159–168.
Morais Cabral, J. H., Jackson, A. P., Smith, C. V., Shikotra, N., Maxwell, A. & Liddington, R. C. (1997). *Nature (London)*, **388**, 903–906.
Morris, R. P., Nguyen, L., Gatfield, J., Visconti, K., Nguyen, K., Schnappinger, D., Ehrt, S., Liu, Y., Heifets, L., Pieters, J., Schoolnik, G. & Thompson, C. J. (2005). *Proc. Natl Acad. Sci. USA*, **102**, 12200–12205.
Murshudov, G. N., Vagin, A. A. & Dodson, E. J. (1997). *Acta Cryst.* D**53**, 240–255.
Navaza, J. (1994). *Acta Cryst.* A**50**, 157–163.
Schoeffler, A. J. & Berger, J. M. (2008). *Q. Rev. Biophys.* **41**, 41–101.
Takiff, H. E., Salazar, L., Guerrero, C., Philipp, W., Huang, W. M., Kreiswirth, B., Cole, S. T., Jacobs, W. R. Jr & Telenti, A. (1994). *Antimicrob. Agents Chemother.* **38**, 773–780.
Vagin, A. & Teplyakov, A. (1997). *J. Appl. Cryst.* **30**, 1022–1025.
Veziris, N., Truffot-Pernot, C., Aubry, A., Jarlier, V. & Lounis, N. (2003). *Antimicrob. Agents Chemother.* **47**, 3117–3122.